Eur. Phys. J. Appl. Phys. (2013) 64: 24502
DOI: 10.1051/epjap/2013120447

THE EUROPEAN PHYSICAL JOURNAL
APPLIED PHYSICS

Regular Article

An optimum PML for scattering problems in the time domain*

Axel Modave[1,a], Abelin Kameni[2], Jonathan Lambrechts[3], Eric Delhez[4], Lionel Pichon[2], and Christophe Geuzaine[1]

[1] Department of Electrical Engineering and Computer Science (Institut Montéfiore), Université de Liège, Grande Traverse 10, 4000 Liège, Belgium
[2] Laboratoire de Génie Électrique de Paris, UMR 8507 CNRS, Supelec, Universities Paris VI and Paris XI, 11 rue Joliot Curie, 91192 Gif-sur-Yvette, France
[3] Institute of Mechanics, Materials and Civil Engineering (iMMC), Université Catholique de Louvain-la-Neuve, avenue George Lemaître 4-6, 1348 Louvain-la-Neuve, Belgium
[4] Department of Aerospace and Mechanical Engineering, Université de Liège, Grande Traverse 12, 4000 Liège, Belgium

Received: 5 October 2012 / Received in final form: 30 November 2012 / Accepted: 2 January 2013
Published online: 6 November 2013 –

Abstract. In electromagnetic compatibility, scattering problems are defined in an infinite spatial domain, while numerical techniques such as finite element methods require a computational domain that is bounded. The perfectly matched layer (PML) is widely used to simulate the truncation of the computational domain. However, its performance depends critically on an absorption function. This function is generally tuned by using case-dependent optimization procedures. In this paper, we will present some efficient functions that overcome any tuning. They will be compared using a realistic scattering benchmark solved with the Discontinuous Galerkin method.

1 Introduction

With the increasing use of electrical, electronic and electromagnetic systems, the study of their undesirable interactions and side effects is an important aspect to be considered by the design engineer. In this context, numerical methods are intensively used to solve problems of electromagnetic compatibility (EMC).

Many EMC problems dealing with radiated perturbations are defined on large or infinite spatial domains. When finite element-type numerical methods are used, a major challenge is then to truncate the computational domain without altering too much the accuracy of the solution.

Different techniques have been developed to handle the truncation of the computational domain. The perfectly matched layer (PML) technique, introduced by Bérenger [1], is one of them and is widely used in both frequency and time domains. The idea is to surround the truncated computational domain with a specific layer. Inside it, the physical medium is adapted in such a way that outgoing waves are progressively damped and leave the domain without reflection. To achieve this, the differential equations of the problem are transformed and an absorption function $\sigma(d)$ governing the damping is introduced.

This paper deals with the choice of the function $\sigma(d)$ that is still tricky when numerical methods are used. We present functions that provide good results without any tuning, unlike the commonly used absorption functions that require case-dependent optimization procedures.

A set of PML equations and a nodal Discontinuous Galerkin (DG) method are introduced in Section 2 for a two-dimensional scattering problem in the time domain. Functional forms of σ are presented and compared with case-dependent-optimized polynomial profiles in Section 3. Two examples of scattering applications are finally presented in Section 4.

2 Mathematical and numerical framework

2.1 Scattering problem in unbounded domain

We consider the two-dimensional scattering of waves by an obstacle in an unbounded domain. The transverse magnetic case is treated, where the electric field has only one component in the z-direction, i.e., $\boldsymbol{e} = [0, 0, e_z]$, while the magnetic field is perpendicular to the z-direction, i.e., $\boldsymbol{h} = [h_x, h_y, 0]$.

In order to perform the numerical simulations with a bounded computational domain, the unbounded domain is truncated, and the resulting domain Ω is surrounded by a PML Ω_{pml}. The domain Ω is assumed to be convex. Its boundary Γ must be sufficiently regular. The PML thickness δ is constant.

* Contribution to the Topical Issue "Numelec 2012", Edited by Adel Razek.

[a] e-mail: a.modave@ulg.ac.be

The non-zero components of the fields $\boldsymbol{e}$ and $\boldsymbol{h}$ are governed by Maxwell's equations in Ω. An incident field is prescribed using a total/scattered field approach with transition at Γ (see, e.g., [2], Sect. 5.6). The scattered field formulation is then used in Ω_{pml} while a total field formulation is considered in Ω.

2.2 A general PML for convex truncated domain

In the PML Ω_{pml}, the scattered fields are governed by the modified equations

$$\varepsilon\frac{\partial \boldsymbol{e}}{\partial t} - \nabla\times\boldsymbol{h} = -\varepsilon\left(\sigma-\sigma_\kappa\right)\boldsymbol{q} - \varepsilon\sigma_\kappa\boldsymbol{e}, \tag{1}$$

$$\mu\frac{\partial \boldsymbol{h}}{\partial t} + \nabla\times\boldsymbol{e} = -\mu\left(\sigma-\sigma_\kappa\right)\boldsymbol{t}(\boldsymbol{t}\cdot\boldsymbol{h}) - \mu\sigma_\kappa\boldsymbol{h}. \tag{2}$$

The additional vector field $\boldsymbol{q}$ introduced in equation (1) has only one component along $\boldsymbol{e}_z$, i.e., $\boldsymbol{q} = [0,\ 0,\ q_z]$, and is governed by

$$\varepsilon\frac{\partial \boldsymbol{q}}{\partial t} - \nabla_{\boldsymbol{n}}\times\boldsymbol{h} = -\varepsilon\sigma\boldsymbol{q}, \tag{3}$$

with $\nabla_{\boldsymbol{n}} = [\boldsymbol{n}(\boldsymbol{n}\cdot\nabla)]$. In these equations, $\sigma(d)$ is the absorption function, assumed to be positive in Ω_{pml}, and

$$\sigma_\kappa(\boldsymbol{x}) = \frac{1}{\kappa^{-1}+d}\int_0^d \sigma(r)\mathrm{d}r, \tag{4}$$

where $\mathrm{d}(\boldsymbol{x}) = \mathrm{dist}(\boldsymbol{x},\Gamma)$ is the distance to Γ and $\kappa(\boldsymbol{x})$ is the curvature of Γ at the point closest to $\boldsymbol{x}$. The unit vector fields $\boldsymbol{n}(\boldsymbol{x})$ and $\boldsymbol{t}(\boldsymbol{x})$ give the normal and the tangent directions to Γ, at the same point. The vector field $\boldsymbol{n}$ then gives the stretching direction of the PML.

These equations are built using a procedure similar to the one described by Collino and Monk [3]. Maxwell's equations are firstly written in the frequency domain with curvilinear coordinates. A complex substitution of d is then made (see [3], Sect. 3). Finally, the time-dependent equations (1) and (2) are obtained using an inverse Fourier transform in space and defining the additional equation (3). These equations are equivalent to those given in [3] for the transverse electric mode and a circular truncation boundary.

If $\sigma(d)$ is singular at the outer boundary of the PML, i.e., at $d=\delta$, the solution must satisfy a homogeneous Dirichlet condition on one of the fields for the problem to be well posed. Alternatively, a Neumann condition or even a radiation condition could be implemented to improve the efficiency of the layer. In this paper, a homogeneous Dirichlet condition on $\boldsymbol{h}$ is always prescribed.

2.3 Numerical solution

The equations above are solved using the nodal DG finite element method as described below.

The domain Ω and the PML Ω_{pml} are decomposed into triangular elements. Over each element Ω_e, each non-zero Cartesian component of each field is approached by a sum of Lagrange basis functions, i.e.,

$$u(t,\boldsymbol{x}) \approx u_e^{\text{num}}(t,\boldsymbol{x}) = \sum_n u_{e,n}^{\text{num}}(t)\phi_{e,n}(\boldsymbol{x}), \quad \forall \boldsymbol{x}\in\Omega_e,$$

where u is the considered component, u_e^{num} is its discrete approximation in the element Ω_e, $u_{e,n}^{\text{num}}$ is the value of u_e^{num} at the node n and $\phi_{e,i}$ is the corresponding Lagrange function that is equal to one at the node n and equal to zero at the others. The global numerical solution is then discontinuous at the cell interfaces [4–6].

The numerical scheme is obtained by considering a weak form of the equations. Multiplying the equations (1)–(3) by test functions $\tilde{\boldsymbol{e}}$, $\tilde{\boldsymbol{h}}$ and $\tilde{\boldsymbol{q}}$, integrating the resulting equations over each cell Ω_e and using integration by part, one obtains

$$\int_{\Omega_e}\left[\varepsilon\frac{\partial \boldsymbol{e}}{\partial t}\cdot\tilde{\boldsymbol{e}} - \boldsymbol{h}\cdot(\nabla\times\tilde{\boldsymbol{e}}) - \boldsymbol{S_e}\cdot\tilde{\boldsymbol{e}}\right]\mathrm{d}\Omega_e - \int_{\Gamma_e}[\boldsymbol{n}_e\times\boldsymbol{h}]^{\text{num}}\cdot\tilde{\boldsymbol{e}}\,\mathrm{d}\Gamma_e = 0, \tag{5}$$

$$\int_{\Omega_e}\left[\mu\frac{\partial \boldsymbol{h}}{\partial t}\cdot\tilde{\boldsymbol{h}} + \boldsymbol{e}\cdot(\nabla\times\tilde{\boldsymbol{h}}) - \boldsymbol{S_h}\cdot\tilde{\boldsymbol{h}}\right]\mathrm{d}\Omega_e + \int_{\Gamma_e}[\boldsymbol{n}_e\times\boldsymbol{e}]^{\text{num}}\cdot\tilde{\boldsymbol{h}}\,\mathrm{d}\Gamma_e = 0, \tag{6}$$

$$\int_{\Omega_e}\left[\frac{\partial \boldsymbol{q}}{\partial t}\cdot\tilde{\boldsymbol{q}} - \boldsymbol{h}\cdot(\nabla_{\boldsymbol{n}}\times\tilde{\boldsymbol{q}}) - \boldsymbol{S_q}\cdot\tilde{\boldsymbol{q}}\right]\mathrm{d}\Omega_e + \int_{\Omega_e}\left[\frac{1}{\kappa^{-1}+d}(\boldsymbol{n}\times\boldsymbol{h})\cdot\tilde{\boldsymbol{q}}\right]\mathrm{d}\Omega_e + \int_{\Gamma_e}[(\boldsymbol{n}_e\cdot\boldsymbol{n})(\boldsymbol{n}\times\boldsymbol{h})]^{\text{num}}\cdot\tilde{\boldsymbol{q}}\,\mathrm{d}\Gamma_e = 0, \tag{7}$$

where $\boldsymbol{S_e}$, $\boldsymbol{S_h}$ and $\boldsymbol{S_q}$ are the right-hand sides of the equations (1)–(3), Γ_e is the boundary of the cell Ω_e and $\boldsymbol{n}_e$ is the exterior normal to Γ_e. The fields are discontinuous at the interfaces between adjacent cells. The values at the two sides of a given interface are both considered to compute the boundary terms. For equations (5) and (6), the two following options are used:

1. A centered discretization, i.e.,

$$[\boldsymbol{n}_e\times\boldsymbol{h}]^{\text{num}} = \frac{\boldsymbol{n}_e\times\{Z\boldsymbol{h}\}}{\{Z\}},$$

$$[\boldsymbol{n}_e\times\boldsymbol{e}]^{\text{num}} = \frac{\boldsymbol{n}_e\times\{Y\boldsymbol{e}\}}{\{Y\}}.$$

2. An upwind discretization, i.e.,

$$[\boldsymbol{n}_e\times\boldsymbol{h}]^{\text{num}} = \frac{\boldsymbol{n}_e\times\{Z\boldsymbol{h}\}}{\{Z\}} - \frac{1}{\{Z\}}\boldsymbol{n}_e\times(\boldsymbol{n}_e\times[\![\boldsymbol{e}]\!]),$$

$$[\boldsymbol{n}_e\times\boldsymbol{e}]^{\text{num}} = \frac{\boldsymbol{n}_e\times\{Y\boldsymbol{e}\}}{\{Y\}} + \frac{1}{\{Y\}}\boldsymbol{n}_e\times(\boldsymbol{n}_e\times[\![\boldsymbol{h}]\!]),$$

while a Lax-Friedrichs discretization is considered for the last equation (7), i.e.,

$$[(\boldsymbol{n}_e \cdot \boldsymbol{n})(\boldsymbol{n} \times \boldsymbol{h})]^{\text{num}} = (\boldsymbol{n}_e \cdot \boldsymbol{n}) \frac{\boldsymbol{n} \times \{Z\boldsymbol{h}\}}{\{Z\}} - c[\![\boldsymbol{q}]\!],$$

where c, Y and Z are the phase velocity, the admittance and the impedance of the medium. $\{u\} = (u^+ + u^-)/2$ and $[\![\boldsymbol{h}]\!] = (u^+ - u^-)/2$ are the mean and the jump of the quantity u at the interface. The superscript "$-$" corresponds to the interior value, while "+" is for the exterior value [6].

The spatial integration scheme is obtained by injecting the discrete fields in the equations and using a numerical integration. The time stepping is made with the Crank-Nicholson method.

3 Absorption functions

The success of the PML technique is mainly due to the perfectly matching property at the interface between the PML medium and the physical domain in the continuous context. It ensures the perfect transmission of waves from one medium to the other without reflection. Moreover, for a PML with a finite thickness δ, reflections are avoided if σ is singular at the outer boundary of the PML (see [7] or [8]). However, this condition does not apply to discrete contexts (e.g., after discretization by finite elements) and the perfect matching is not ensured.

When numerical methods are used, the properties of the PML depend critically on σ, on the thickness δ and on the discretization. The continuous properties of the PML can be nearly recovered by taking a large thickness δ or by using a very accurate discretization with a fine mesh or high-order elements. This approach is however not feasible because it induces a substantial increase of the computational cost.

The function $\sigma(d)$ is the most crucial parameter. Indeed, the performance of the PML decreases dramatically when the damping of the solution induced by large values of σ cannot be captured by the discretization grid [9]. Therefore, σ must be chosen in such a way as to introduce enough damping of outgoing waves without inducing a too sharp decrease of the fields in the PML. Polynomial profiles of σ allow such a progressive damping:

$$\sigma_p(d) = \alpha \left(\frac{d}{\delta}\right)^n, \tag{8}$$

with $n > 0$ and where α is the value of the absorption function at the outer side of the layer. This profile is widely used (see, e.g., [7,8,10,11]). However, no general rule exists to choose the parameters α and n. Therefore, they are usually tuned using expensive and case-dependent optimization procedures. As an alternative, hyperbolic profiles have been proposed by Bermúdez et al. [7]:

$$\sigma_{\text{h}}(d) = \frac{\alpha}{(\delta - d)^n}, \tag{9}$$

$$\sigma_{\text{sh}}(d) = \frac{\alpha}{(\delta - d)^n} - \frac{\alpha}{\delta^n}, \tag{10}$$

with again two free dimensionless parameters: α and n. Fortunately, these two profiles do not require any tuning with $n = 1$. Bermúdez et al. [7] show in a continuous finite element context with a straight Cartesian PML and time-harmonic equations that the solution is indeed close to the optimum when α is equal to the propagation velocity of the medium. We extended this result to the finite difference and the DG contexts with the time-dependent equations in [9,12].

4 Numerical simulations

We show in this section that the results of the previous works [7,9,12] are still valid for more realistic scattering benchmarks.

4.1 Scattering by a cavity with an aperture

Consider the scattering by the perfectly conducting cavity studied by Ojeda and Pichon [13] in the time-harmonic context. This cavity is rectangular (600 mm × 400 mm) of

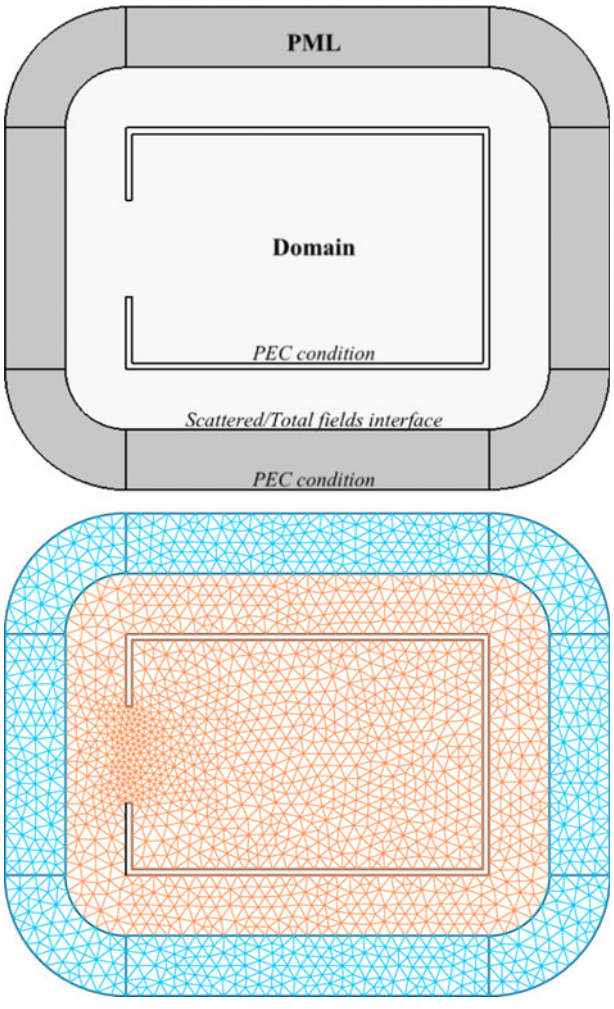

Fig. 1. Geometry and mesh of the first benchmark.

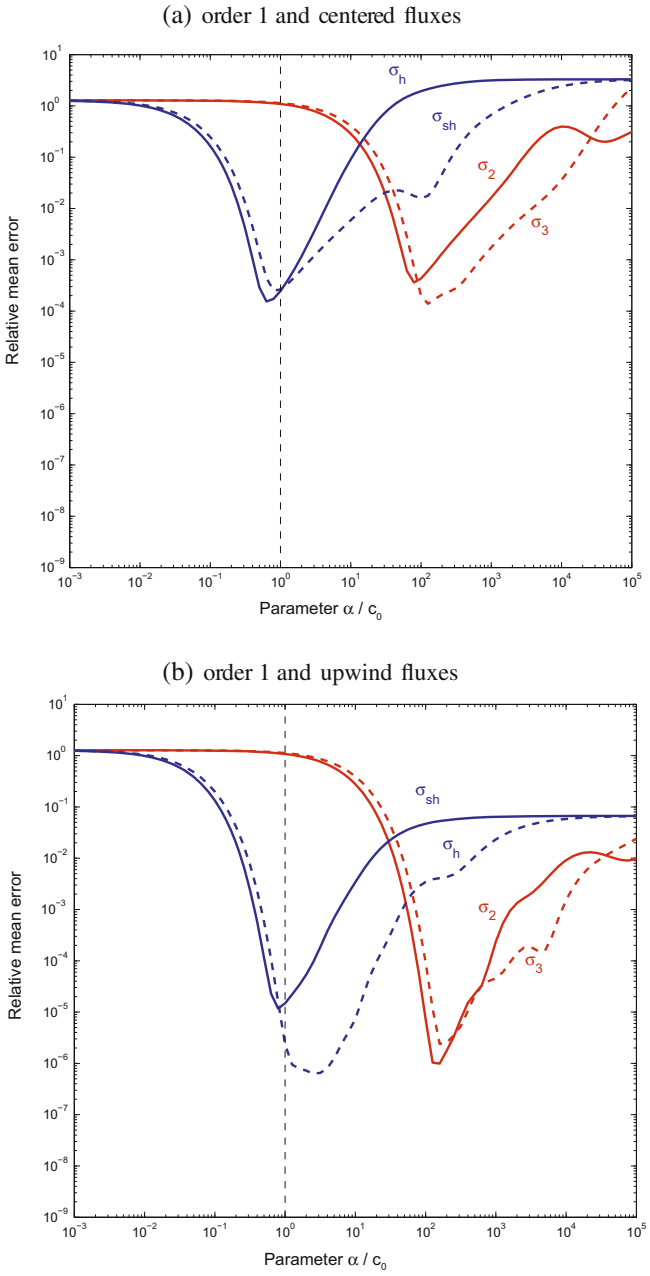

Fig. 2. Relative mean error as a function of α with the different absorption functions for the first benchmark. Elements of order 1 are used with centered (a) or upwind numerical fluxes (b). Vertical lines indicate $\alpha = c_0$.

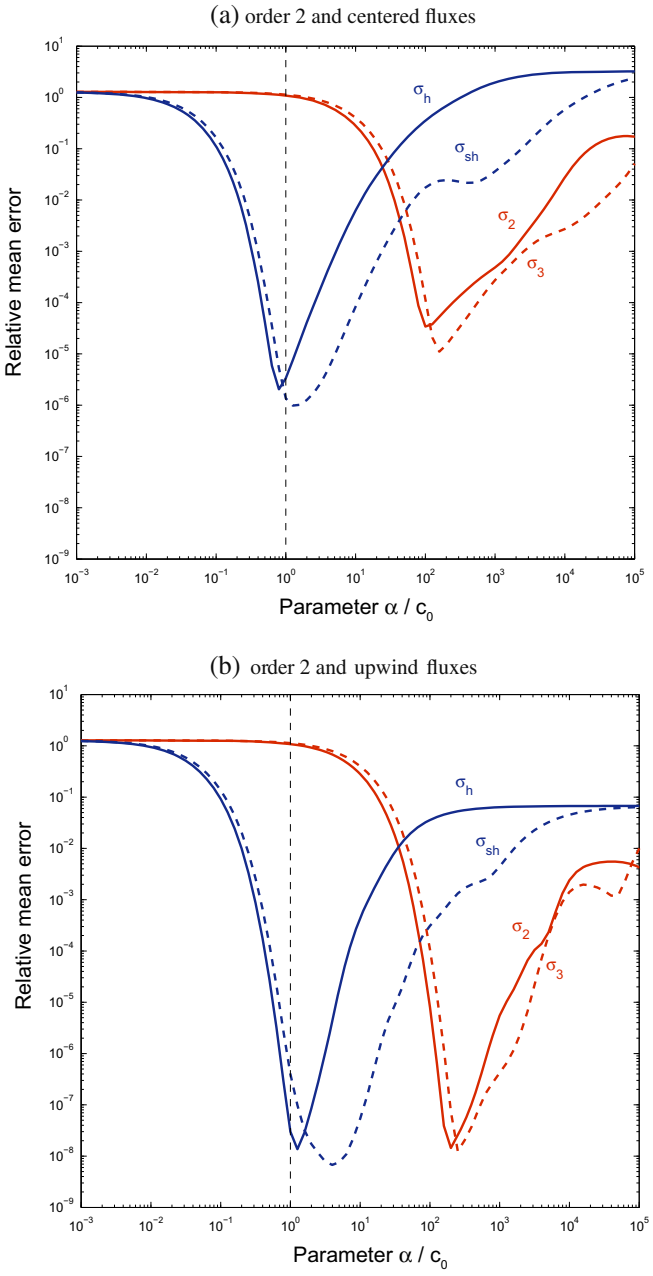

Fig. 3. Relative mean error as a function of α with the different absorption functions for the first benchmark. Elements of order 2 are used with centered (a) or upwind numerical fluxes (b). Vertical lines indicate $\alpha = c_0$.

thickness 20 mm with an aperture of 160 mm in the middle of the left side (Fig. 1). The truncated computational domain is rectangular with rounded corners, surrounded by a PML of thickness $\delta = 0.2$ m. A Gaussian pulse is prescribed with the incident field, i.e.,

$$\boldsymbol{e}^i = E^i \sqrt{\frac{\mu_0}{\varepsilon_0}} \exp\left[-\left(\frac{(x-x_0)-c_0 t}{\ell}\right)^2\right] \hat{\boldsymbol{z}}, \qquad (11)$$

with $x_0 = -1200$ mm, $\ell = 50$ mm, $c_0 = 1/\sqrt{\mu_0 \varepsilon_0}$ and $E^i = 0.5\sqrt{\mu_0/\varepsilon_0}$. It describes a pulse coming from the left side of the domain and propagating to the right. The final time of the simulation is $T = 250\Delta t$, with the time step $\Delta t = 510^{-11}$ s.

The efficiency of the PML is quantified by computing the relative mean error of the simulation, i.e.,

$$\frac{\int_0^T \int_\Omega \left(\frac{\varepsilon_0}{2} \|\boldsymbol{e} - \boldsymbol{e}_{\text{ref}}\|^2 + \frac{\mu_0}{2} \|\boldsymbol{h} - \boldsymbol{h}_{\text{ref}}\|^2\right) \mathrm{d}\Omega \mathrm{d}t}{\int_0^T \int_\Omega \left(\frac{\varepsilon_0}{2} \|\boldsymbol{e}_{\text{ref}}\|^2 + \frac{\mu_0}{2} \|\boldsymbol{h}_{\text{ref}}\|^2\right) \mathrm{d}\Omega \mathrm{d}t}, \qquad (12)$$

where $\boldsymbol{e}_{\text{ref}}$ and $\boldsymbol{h}_{\text{ref}}$ are reference fields computed with a larger computational domain. Figures 2 and 3 show this relative mean error as a function of α for different absorption functions: parabolic σ_2, cubic σ_3, hyperbolic σ_{h} (with $n = 1$) and shifted-hyperbolic σ_{sh} (with $n = 1$).

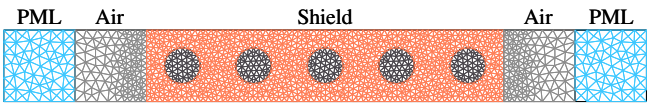

Fig. 4. Geometry and mesh of the second benchmark.

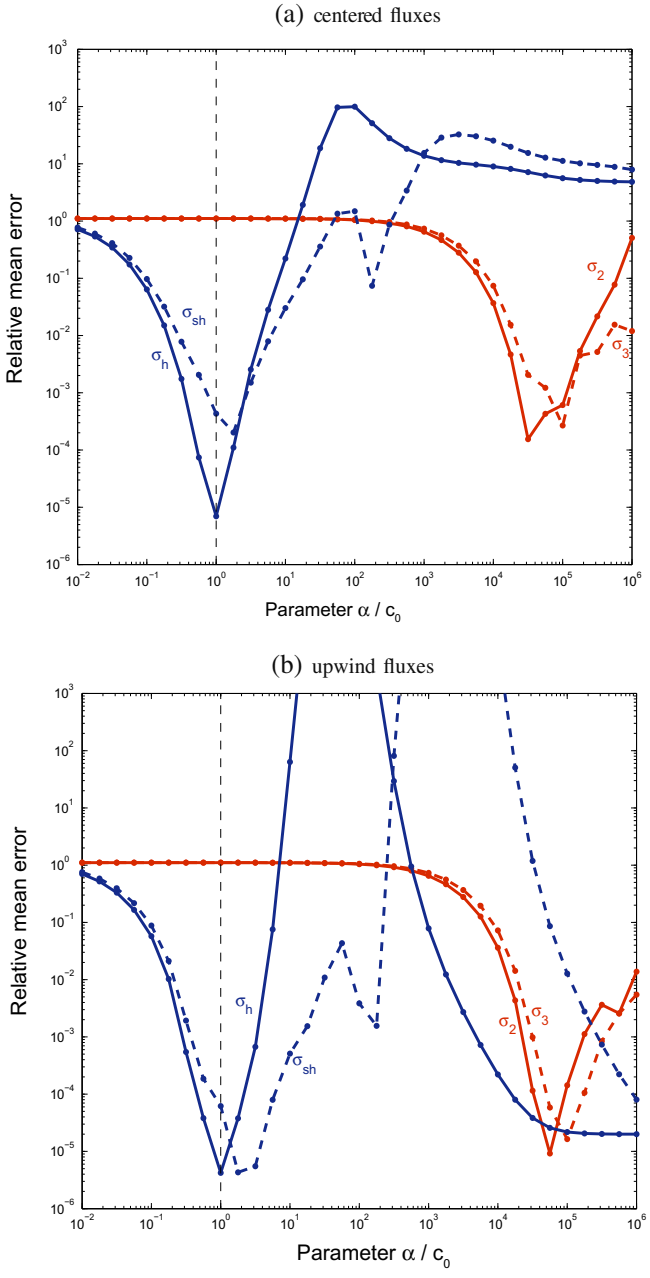

Fig. 5. Relative mean error as a function of α with the different absorption functions for the second benchmark. Elements of order 1 are used with centered (a) or upwind numerical fluxes (b). Vertical lines indicate $\alpha = c_0$.

For each case, the different absorption functions considered in this numerical experiment give equivalent results when they are optimized, i.e., at the minimum of the curves of Figures 2 and 3, except the hyperbolic function σ_{h} that does not perform so well at order 1 with upwind numerical fluxes.

The smallest error with σ_{h} and σ_{sh} is always obtained with a value of α close to the propagation velocity c_0.

4.2 Scattering by an electromagnetic shield

As a second application, consider the scattering of a plane wave by the wall represented in Figure 4. The wall is made of a non-conducting medium and is filled with circular conducting inclusions stored in squared form. The thickness of the wall is 1 mm and the surfacic inclusion rate is $\tau = 20\%$. The permittivity is $5\varepsilon_0$ in the non-conducting medium and ε_0 in the inclusions. The permeability is μ_0 throughout the wall. The conductivity of the inclusions is 10^3 S/m.

In this problem, we are not interested in the electromagnetic field in the air. Therefore, two PMLs are directly put against the walls. In this simulation, the incident field (11) is prescribed at the interface between the left PML and the wall using a total/scattered field transition, with $x_0 = -5$ mm, $\ell = 1$ mm and $E^i = 0.01\sqrt{\mu_0/\varepsilon_0}$. Reflected waves are damped in the left PML, while the right PML absorbs transmitted waves.

The relative mean error (12), where the integration is carried out over the shield and the air layers, is plotted in Figure 5. The duration of the simulation and the time step are $T = 3000\,\Delta t$ and $\Delta t = 410^{-14}$ s, respectively.

The curves confirm the conclusions obtained with the previous benchmark. The optimum α is close to c_0 for hyperbolic functions just like for the first test case. While an optimum value can also be identified for polynomial profiles, this value differs significantly from the optimum value found for the cavity problem. It differs also from the optimum values identified in previous works.

5 Conclusion

A set of PML equations have been presented for two-dimensional scattering EMC problem in the time domain, to simulate a two-dimensional convex truncation boundary. The computational domain could then be reduced to decrease the computational cost.

Concerning the absorption function $\sigma(d)$, the results of this paper are coherent with those of previous works [7,9,12]: hyperbolic and shifted-hyperbolic functions (9) and (10) can be used with $\alpha = c$ and $n = 1$. They are efficient, without any case-dependent costly tuning. By contrast, while polynomial profiles perform equally well, the optimum values of the corresponding coefficients are strongly case dependent and cannot be set on physical grounds only. The hyperbolic and shifted-hyperbolic profiles are therefore potentially much better

suited to large-scale industrial EMC problems, e.g., three-dimensional simulations of the shielding effectiveness of complex structures.

This work was supported in part by the Belgian Science Policy (IAP P6/21 and P7), Belgian French Community (ARC 09/14-02) and Walloon Region (WIST3 No. 1017086 "ONELAB"). Jonathan Lambrechts is a Postdoctoral Researcher with the Belgian National Fund for Scientific Research (FNRS).

References

1. J.P. Bérenger, J. Comput. Phys. **114**, 185 (1994)
2. A. Taflove, S.C. Hagness, *Computational Electrodynamics: The Finite-Difference Time-Domain Method*, 3rd edn. (Artech House, Boston, 2005)
3. F. Collino, P.B. Monk, SIAM J. Sci. Comput. **19**, 2061 (1998)
4. G. Cohen, X. Ferrieres, S. Pernet, J. Comput. Phys. **217**, 340 (2006)
5. L. Fezoui, S. Lanteri, S. Lohreng, S. Piperno, Math. Model. Numer. Anal. **39**, 1149 (2005)
6. J.S. Hesthaven, T. Warburton, J. Comput. Phys. **181**, 186 (2002)
7. A. Bermúdez, L. Hervella-Nieto, A. Prieto, R. Rodríguez, SIAM J. Sci. Comput. **30**, 312 (2007)
8. F. Collino, P.B. Monk, Comput. Methods Appl. Mech. Eng. **164**, 157 (1998)
9. A. Modave, E. Deleersnijder, E.J.M. Delhez, Ocean Dyn. **60**, 65 (2010)
10. J.P. Bérenger, *Perfectly Matched Layer (PML) for Computational Electromagnetics* (Morgan & Claypool, 2007)
11. S. Gedney, in *Computational Electrodynamics: The Finite-Difference Time-Domain Method*, edited by A. Taflove (Artech House, 2005), pp. 273–328
12. A. Modave, E.J.M. Delhez, C. Geuzaine, in *Proceedings of the 10th International Conference on Mathematical and Numerical Aspects of Waves Propagation, Vancouver, Canada, 2011*, pp. 591–594
13. X. Ojeda, L. Pichon, J. Electromagn. Waves Appl. **19**, 1375 (2005)